

1 **A comprehensive study about the in-cloud processing of nitrate through**  
2 **coupled measurements of individual cloud residuals and cloud water**

3

4 Guohua Zhang<sup>1,2,3</sup>, Xiaodong Hu<sup>1,2,4</sup>, Wei Sun<sup>1,2,4</sup>, Yuxiang Yang<sup>1,2</sup>, Ziyong Guo<sup>1,2,4</sup>, Yuzhen Fu<sup>1,2</sup>, Haichao  
5 Wang<sup>5</sup>, Shengzhen Zhou<sup>5</sup>, Lei Li<sup>6</sup>, Mingjin Tang<sup>1,2,3</sup>, Zongbo Shi<sup>7</sup>, Duohong Chen<sup>8</sup>, Xinhui Bi<sup>1,2,3,\*</sup>, Xinming  
6 Wang<sup>1,2,3</sup>

7

8 <sup>1</sup> State Key Laboratory of Organic Geochemistry and Guangdong Provincial Key Laboratory  
9 of Environmental Protection and Resources Utilization, Guangzhou Institute of  
10 Geochemistry, Chinese Academy of Sciences (CAS), Guangzhou 510640, PR China

11 <sup>2</sup> CAS Center for Excellence in Deep Earth Science, Guangzhou, 510640, China

12 <sup>3</sup> Guangdong-Hong Kong-Macao Joint Laboratory for Environmental Pollution and Control,  
13 Guangzhou Institute of Geochemistry, CAS, Guangzhou 510640, PR China

14 <sup>4</sup> University of Chinese Academy of Sciences, Beijing 100049, PR China

15 <sup>5</sup> School of Atmospheric Sciences, Sun Yat-sen University, Guangzhou 519082, PR China

16 <sup>6</sup> Institute of Mass Spectrometer and Atmospheric Environment, Jinan University,  
17 Guangzhou 510632, PR China

18 <sup>7</sup> School of Geography, Earth and Environmental Sciences, University of Birmingham,  
19 Birmingham B15 2TT, U.K.

20 <sup>8</sup> State Environmental Protection Key Laboratory of Regional Air Quality Monitoring,  
21 Guangdong Environmental Monitoring Center, Guangzhou 510308, PR China

22

23 Corresponding author: Xinhui Bi ([bixh@gig.ac.cn](mailto:bixh@gig.ac.cn))

24

25 **Key points**

- 26 ● We show the direct observational evidence for the enhanced nitrate formation in the  
27 cloud water and residual particles.
- 28 ● The variation of in-cloud nitrate could be well predicted by the  $[\text{NO}_x][\text{O}_3]$ , droplets'  
29 surface area, and temperature.
- 30 ● Hydrolysis of  $\text{N}_2\text{O}_5$  served as a potentially important route for the in-cloud formation of  
31 nitrate even during the daytime.
- 32

---

**33 Abstract**

34 Nitrate aerosol has become an increasingly important component of fine particles. While  
35 the formation and evolution of nitrate in airborne particles are extensively investigated, little  
36 is known about the formation of nitrate in clouds. Here we present a detailed investigation  
37 on the in-cloud formation of nitrate based on the size-resolved mixing state of nitrate in the  
38 individual cloud residual and cloud-free particles by single particle mass spectrometry, and  
39 the mass concentrations of nitrate in the cloud water and PM<sub>2.5</sub> at a mountain site (1690 m  
40 a.s.l.) in southern China. The results show a significant enhancement of nitrate mass fraction  
41 in cloud water and relative intensity of nitrate in the mass spectra of the cloud residual  
42 particles, underlining a critical role of in-cloud processing in the formation of nitrate. Based  
43 on the size distribution of relative intensity of nitrate in individual particles, we exclude the  
44 gas phase scavenging of HNO<sub>3</sub> and the facilitated activation of nitrate-containing particles  
45 as the major contribution for the enhanced nitrate. Regression analysis and theoretical  
46 calculations further reveal that nitrate is highly related ( $R^2 = \sim 0.6$ ) to the variation of  
47 [NO<sub>x</sub>][O<sub>3</sub>], temperature and droplet surface area in clouds. Accounting for droplet surface  
48 area greatly enhances the predictability of the observed nitrate compared with using  
49 [NO<sub>x</sub>][O<sub>3</sub>] and temperature. Our results indicate a critical role of in-cloud formation of  
50 nitrate via N<sub>2</sub>O<sub>5</sub> hydrolysis, even during the daytime, attributed to the diminished light in  
51 clouds. The detailed observation would benefit future investigations of the evolution and  
52 oxidative impacts of nitrate.

53

---

## 54 **1. Introduction**

55 Aerosol nitrate is an increasingly important component of PM<sub>2.5</sub>, in particular,  
56 contributing to haze formation in China (Guo *et al.*, 2014; Wen *et al.*, 2018; Lu *et al.*, 2019;  
57 Tian *et al.*, 2019; Xu *et al.*, 2019; Fu *et al.*, 2020; Liu *et al.*, 2020b; Zheng *et al.*, 2020). As a  
58 key inorganic component in cloud water, nitrate can also modify microphysical properties  
59 of cloud, influence aqueous-phase processes in droplets and affect ecosystem after wet  
60 deposition (Schneider *et al.*, 2017). Notably, aerosol nitrate is an important product in the  
61 cycling of odd nitrogen (Chang *et al.*, 2011; Huang *et al.*, 2018; Zheng *et al.*, 2020; Zhang  
62 *et al.*, 2021), playing significant roles in tropospheric ozone and OH production (Scharko *et*  
63 *al.*, 2014; Kaur and Anastasio, 2017; Ye *et al.*, 2017a; Ye *et al.*, 2017b), and contributing to  
64 net aerosol composition and radiative forcing (Bauer *et al.*, 2007; Xu and Penner, 2012;  
65 Hauglustaine *et al.*, 2014).

66 Aerosol nitrate originates from the oxidation of NO<sub>x</sub>, which refers to gas phase  
67 oxidation of NO<sub>2</sub> by the hydroxyl radical (OH) and then condensation (daytime chemistry)  
68 and the hydrolysis of N<sub>2</sub>O<sub>5</sub> (nighttime chemistry) to nitrate in aqueous particles, initiated by  
69 the oxidation of NO<sub>2</sub> by ozone (O<sub>3</sub>) to produce the NO<sub>3</sub> radical (Seinfeld and Pandis, 2006).  
70 In contrary to aerosol sulfate formation, which is dominated by aqueous phase reactions,  
71 both gas phase oxidation and the hydrolysis of N<sub>2</sub>O<sub>5</sub> represent the major processes forming  
72 nitrate aerosols (Chen *et al.*, 2020; Xiao *et al.*, 2020). The formation mechanism and the  
73 associated controlling factors of aerosol nitrate at the ground level have been extensively  
74 investigated. Apart from precursors and oxidants, the formation and evolution of nitrate

75 depend on the availability of ammonia ( $\text{NH}_3$ ) as well as environment conditions (e.g.,  
76 temperature (T), relative humidity (RH)), and the presence of other ionic species in  
77 particulate phase (*Chen et al.*, 2018; *Shi et al.*, 2019; *Chen et al.*, 2020; *Fan et al.*, 2021; *Lin*  
78 *et al.*, 2021).

79 Comparatively, detailed observational investigations and the possible mechanisms  
80 governing nitrate behavior upon in-cloud processes are scarce, although it is well-known  
81 that clouds play an important role in the transport and transformation of tropospheric  
82 pollutants (*Ervens*, 2015; *McNeill*, 2017; *Li et al.*, 2020b). *Drewnick et al.* (2007) and  
83 *Prabhakar et al.* (2014) reported that the relatively enhanced nitrate in clouds was associated  
84 with the composition of the activating cloud condensation nuclei (CCN), rather than  
85 preferential scavenging of nitric acid ( $\text{HNO}_3$ ) in clouds. Differently, there are also studies  
86 highlighting the predominant role of nitric acid partitioning in nitrate formation in clouds, in  
87 contrary to nucleation scavenging of sulfate (*Leaitch et al.*, 1988; *Hayden et al.*, 2008;  
88 *Schneider et al.*, 2017). *Hayden et al.* (2008) also noted that potential contributions from  
89 gas-phase  $\text{N}_2\text{O}_5$  cannot be ruled out. However, the relative role of in-situ formation of nitrate  
90 in clouds remains poorly quantified, and the controlling factors remain unclear. Therefore,  
91 more detailed investigations are required to integrate the role of cloud in processing of nitrate  
92 in the troposphere.

93 The aim of this study is to illustrate the in-cloud formation mechanisms of nitrate and  
94 evaluate the relative contribution of each pathway to nitrate in cloud water for daytime and  
95 nighttime. To this aim, the mixing state of individual cloud residual, interstitial and cloud-

96 free particles were measured in high-time resolution with a single particle aerosol mass  
97 spectrometer (SPAMS). The combination of a counter flow virtual impactor (CVI) and  
98 aerosol mass spectrometry (including SPAMS) allows for the high-time resolved  
99 observations of size and chemical compositions of submicron cloud RES particles (*Hao et*  
100 *al.*, 2013; *Boone et al.*, 2015; *Lin et al.*, 2017; *Zhang et al.*, 2017). In addition, cloud water  
101 and PM<sub>2.5</sub> samples were collected, and the chemical compositions were measured to provide  
102 additional quantitative evidence.

103

## 104 **2. Experimental section**

### 105 **2.1 Aerosol and cloud measurements**

106 Aerosol and cloud measurements were performed at the Mt. Tianjing site (24°41'56"N,  
107 112°53'56"E, 1690 m a.s.l.) in southern China, as described in detail by *Lin et al.* (2017),  
108 during 9 May – 4 June 2018 and 13 November – 9 December 2020. Cloud events can be  
109 distinguished by a sudden drop of visibility (to < ~1 km) and a sharp increase of relative  
110 humidity (RH) to > 95%, as record by sensors equipped with a ground-based counterflow  
111 virtual impactor (GCVI) (Model 1205, Brechtel Mfg. Inc., USA) (*Lin et al.*, 2017). Overall,  
112 nineteen cloud events (lasting more than six hours) were identified for 2018 spring and ten  
113 for 2020 winter, as also marked in Fig. S1. The visibility was generally lower than 0.1 km  
114 during the cloud events, versus as high as 80 km during cloud-free periods. Besides a  
115 relatively long cloud event throughout 9 – 12 May, the cloud events were typically observed  
116 during nighttime for 2018 spring, associated with a prominently diurnal variation of RH and

117 visibility. The RH during the daytime ranged between 70-80%, and raised to > 95% during  
118 nighttime. The duration of cloud events was in a range of 6-24 hours for 2020 winter. Air  
119 masses from the southern continental and marine areas dominated over the 2018 spring,  
120 versus southwestern continental areas over the 2020 winter (Fig. S2), obtained by HYSPLIT  
121 4.9 (<http://ready.arl.noaa.gov/HYSPLIT.php>) (Draxler and Rolph, 2012).

122 An incorporation of counterflow virtual impactor (CVI) or GCVI allows the separation  
123 of interstitial gases and aerosols from cloud droplets that are evaporated to obtain the cloud  
124 RES particles (Pratt *et al.*, 2009; Bi *et al.*, 2016; Roth *et al.*, 2016). Briefly, the GCVI was  
125 applied to collect the cloud droplets with predefined size (7.5-8.5  $\mu\text{m}$  in the present study)  
126 with the cloud RES particles as output after dried in the evaporation chamber (with an air  
127 flow temperature at 40 °C) (Shingler *et al.*, 2012). The influence of cloud-free air can be  
128 negligible as the number concentration of GCVI output particles was measured to be  $\sim 1 \text{ cm}^{-3}$   
129  $^3$ , but at a magnitude of  $\sim 10^3 \text{ cm}^{-3}$  in the cloud-free air. In the present study, the number  
130 concentration of the cloud RES particles sampled during the cloud events was at a level of  
131  $\sim 100 \text{ cm}^{-3}$  on average. In addition, a  $\text{PM}_{2.5}$  inlet was used to deliver cloud INT particles  
132 during cloud events or cloud-free particles.

133

## 134 **2.2 SPAMS measurements and data processing**

135 A SPAMS (Hexin Analytical Instrument Co., Ltd., Guangzhou, China), an Aethalometer  
136 (AE-33, Magee Scientific Inc.), and a scanning mobility particle sizer (SMPS; MSP  
137 Cooperation) were deployed to characterize the physical and chemical properties of the

138 sampled particles. The instruments were connected downstream the GCVI or PM<sub>2.5</sub> inlets.  
139 Cloud RES and cloud INT particles were alternately sampled with an interval of ~1 h during  
140 some randomly selected cloud events. When there is no cloud, these instruments were  
141 connected to the PM<sub>2.5</sub> inlet in order to measure the cloud-free particles. In the present study,  
142 aerosol surface area (SA) for cloud-free particles were directly calculated from the size  
143 distribution data obtained from SMPS, whereas it can only be estimated based on the same  
144 data for the cloud residues assuming a mean droplet size at 7  $\mu\text{m}$ . We recognize the possible  
145 uncertainty, but the estimated SA should correlate with real values and thus does not affect  
146 our conclusions.

147 The vacuum aerodynamic diameter ( $d_{va}$ ) and mass spectral information for individual  
148 particles could be obtained by the SPAMS (Li *et al.*, 2011). A brief description on the  
149 performance of the SPAMS can also be found in the Supplement. Over the sampling period  
150 for 2018 spring and 2020 winter, a respective ~20, 000, 000 particles with mass spectral  
151 information were analyzed, using the FATEs toolkit based on Matlab (The MathWorks, Inc.)  
152 (Sultana *et al.*, 2017). The particles were classified by an adaptive resonance theory-based  
153 neural network algorithm (Song *et al.*, 1999), with the inputs of ion peak intensities. Seven  
154 types with distinct mass spectral characteristics (Fig. S3), accounting for > 95% of all the  
155 detected particles, were obtained for further analysis. Defined as fractional peak area of each  
156 m/z relative to the sum of peak areas in a mass spectrum, relative peak area (RPA) is  
157 generally applied to represent the relative amount of a species within a particle (Jeong *et al.*,  
158 2011; Healy *et al.*, 2013). The presence of nitrate can be identified with ion peaks (defined

159 as five times the noise signal) at  $m/z$  -62  $[\text{NO}_3]^-$  or  $m/z$  -46  $[\text{NO}_2]^-$ . Approximate 70-80% of  
160 all the detected particles in the size range of 100-2000 nm contained nitrate ion signals for  
161 our measurements.

162

### 163 **2.3 Cloud water/PM<sub>2.5</sub> collection and chemical analysis**

164 A Caltech Active Strand Cloud Water Collector (CASCC2) was applied to collect cloud  
165 water (with droplet size  $> 3.5 \mu\text{m}$ ). The average cloud liquid water content (LWC) for each  
166 sampling period can be derived from the equation:  $\text{LWC} = \Delta m / (\Delta t \times \eta \times Q)$ , based on each  
167 sample mass ( $\Delta m$ ), duration time ( $\Delta t$ ), flow rate ( $Q = 5.8 \text{ m}^3 \text{ min}^{-1}$ ), and collection efficiency  
168 ( $\eta = 86\%$ ).

169 A total of 58 / 53 cloud water samples were collected over the nineteen / ten cloud events  
170 for 2018 spring and 2020 winter, respectively, with the duration time ranging between 2 and  
171 10 hours. The pH for collected samples were immediately measured using a pH meter  
172 (Mettler Toledo, Switzerland) after filtered through a  $0.22 \mu\text{m}$  filter, followed by kept at -  
173  $20 \text{ }^\circ\text{C}$  until the analysis.

174 PM<sub>2.5</sub> samples were collected on quartz filters using a PM<sub>2.5</sub> sampler (PM-PUF-300,  
175 Mingye Instruments, China) at a flow rate of  $300 \text{ L min}^{-1}$ . The filter were pre-conditioned in  
176  $450 \text{ }^\circ\text{C}$  for 6 hours to eliminate the potential influence of organics. In total, 20 / 36 PM<sub>2.5</sub>  
177 samples were collected for the 2018 spring and 2020 winter, respectively. The samples were  
178 kept at  $-20 \text{ }^\circ\text{C}$  immediately until further analysis. These samples are representative for the  
179 cloud-free particles or cloud INT particles during cloud events.

180 Cloud water and PM<sub>2.5</sub> samples were analyzed with ion chromatograph (Metrohm 883  
181 IC plus, Switzerland) for water soluble inorganic ions (Na<sup>+</sup>, NH<sub>4</sub><sup>+</sup>, K<sup>+</sup>, Ca<sup>2+</sup>, Mg<sup>2+</sup>, Cl<sup>-</sup>, NO<sub>3</sub><sup>-</sup>,  
182 and SO<sub>4</sub><sup>2-</sup>) and total organic carbon analyzer (Vario, Elementar, Germany for 2018 samples  
183 and TOC-V, Shimadzu, Japan for 2020 samples) for water soluble organic carbon (WSOC).  
184 The overall uncertainty for the concentration of each species is calculated to be < 15% based  
185 on parallel analyses. The nitrate mass fractions in cloud water and PM<sub>2.5</sub> were calculated by  
186 dividing the nitrate concentration by the sum of the measured water-soluble inorganic ions  
187 and water-soluble organic matter (estimated by 1.6\*WSOC).

188

#### 189 **2.4 Box modeling of nitrate formation in cloud**

190 A multiphase chemical box model (RACM-CAPRAM) was used to explain the nitrate  
191 formation mechanisms. The model is and constrained by observations. It couples the  
192 regional atmospheric chemistry mechanism version 2 (RACM2; including 363 chemical  
193 reactions) and the chemical aqueous-phase radical mechanism version 2.4 (CAPRAM2.4;  
194 including 438 chemical reactions) to account for gas- and aqueous-phase atmospheric  
195 chemistry (Ervens *et al.*, 2003; Wen *et al.*, 2018). This model has been utilized previously to  
196 simulate the nighttime nitrate formation in Beijing and Shanghai (Pathak *et al.*, 2009).

197 The average concentration of NO<sub>2</sub> (~25 ppb) and O<sub>3</sub> (~100 ppb) for gas-phase precursors  
198 and LWC (0.1 g m<sup>-3</sup>) for cloud droplets, obtained from the in-situ measurements, were taken  
199 as representative parameters for the atmosphere condition at Mt. Tianjing, and used as initial  
200 conditions for model simulation. The detailed initial conditions for the model are listed in

201 the SI Table S1. Several comparisons through varying the LWC and photolysis rate were  
202 considered in order to investigate the role of LWC and photolysis on the formation of nitrate  
203 in the cloud. Three major pathways for nitrate formation are considered in this model: (1)  
204 The oxidation of  $\text{NO}_2$  by the OH radical produces  $\text{HNO}_3$  and partitioning of gaseous  $\text{HNO}_3$   
205 into the aqueous phase; (2) The hydrolysis reactions of  $\text{N}_2\text{O}_5$ ; and (3) The aqueous-phase  
206 reactions of  $\text{NO}_3$  radicals.

207

### 208 **3. Results and discussion**

#### 209 **3.1. Enhanced in-cloud production of nitrate**

210 Figure 1 shows the statistical results of the nitrate mass fractions in cloud water and  
211  $\text{PM}_{2.5}$  and the hourly average RPA of nitrate in the cloud-free, cloud residual, and cloud  
212 interstitial particles. It can be seen that the mass fraction of nitrate in cloud water (~20% on  
213 average) is obviously higher than those in  $\text{PM}_{2.5}$  (< 15% on average) during cloud-free  
214 periods and cloud events for both 2018 spring and 2020 winter. Consistently, RPA of nitrate  
215 was substantially enhanced in the cloud INT particles and particularly cloud residues,  
216 relative to the cloud-free particles. The influence of air mass on the enhanced nitrate can be  
217 ruled out for 2018 spring as they similarly originated from southern areas over the whole  
218 campaign period (Fig. S2). While the air masses originated from several regions during 2020  
219 winter, they did not show the difference between cloud-free periods and cloud events (Fig.  
220 S2). Therefore, such enhancement points to the in-situ formation, preferential uptake of nitric  
221 acid and/or scavenging of nitrate-rich particles during cloud processing.

222 There are several pathways that might contribute to the enhanced nitrate in cloud  
223 droplets, including (1) the scavenging of gas-phase HNO<sub>3</sub>, (2) the preferential activation of  
224 nitrate-rich particles, and (3) in-cloud aqueous production of nitrate via reaction of NO<sub>3</sub>  
225 radicals or hydrolysis of N<sub>2</sub>O<sub>5</sub> (*Sellegri et al.*, 2003; *Fahey et al.*, 2005; *Hayden et al.*, 2008).  
226 The mechanism via the dissolution of NO<sub>2</sub> and its aqueous phase oxidation is relatively slow  
227 and unlikely to be a significant source of cloud water nitrate (*Seinfeld and Pandis*, 2006).

228 We first exclude the scavenging of gas-phase HNO<sub>3</sub> as a major pathway through the  
229 analysis of size distribution of nitrate RPA and RPA ratio (nitrate/sulfate), although all gas  
230 phase HNO<sub>3</sub> could be scavenged and present in the aqueous phase in a typical cloud with  
231 LWC > 0.1 g m<sup>-3</sup> (*Seinfeld and Pandis*, 2006). As can be seen in Fig. 2, the RPA of nitrate  
232 and RPA ratios of nitrate/sulfate distributes relatively stable over the measured size range,  
233 which suggests that the gas phase scavenging of HNO<sub>3</sub> is not the dominant pathway in the  
234 present conditions. This is because gas-phase mass transfer would lead to enhanced nitrate  
235 in the smaller droplets with higher total surface area (*Drewnick et al.*, 2007). In contrast,  
236 sulfate is mainly due to nucleation scavenging which, depending on the size distribution of  
237 preexisting aerosols, could result in being shifted toward larger sizes. As also discussed in  
238 the following section, the formation of HNO<sub>3</sub> would be certainly suppressed by the presence  
239 of cloud.

240 We also indicate that the contribution of preferential activation of nitrate-rich particles  
241 should also be limited since such a process would lead to depletion of nitrate in the cloud  
242 interstitial particles relative to the cloud-free particles. But this is not the case, as the RPA of

243 nitrate and RPA ratios of nitrate/sulfate in the cloud interstitial particles are considerably  
244 higher than those in the cloud-free particles (Fig. 2). Both the enhanced nitrate in the cloud  
245 residual and interstitial particles suggest the in-cloud formation of nitrate, although the  
246 variation of RPA cannot provide a quantitative view. The enhancement of nitrate in the cloud  
247 interstitial particles may also indicate that in-cloud condition facilitates the formation of  
248 nitrate even in the inactivated particles. Similar results have also been observed in our  
249 previous study for oxalate. Consistently, the formation of nitrate in the cloud interstitial  
250 particles also grows their size towards the larger mode, i.e., cloud RES particles, compared  
251 with the cloud-free particles (Fig. S4).

252

### 253 **3.2. In-cloud nitrate formation**

254 A theoretical estimation of nitrate production for 2020 winter is performed based on the  
255 well-established kinetic characteristic of reactions between  $\text{NO}_2$  and  $\text{O}_3$  and uptake of  $\text{N}_2\text{O}_5$   
256 onto aerosol/droplet surfaces that formed  $\text{HNO}_3$  (SI text S1), corresponding to the nighttime  
257 chemistry. It is reasonable since the heterogeneous hydrolysis of  $\text{N}_2\text{O}_5$  within aerosol  
258 particles, fog, or cloud droplets has been shown to be much faster than homogeneous  
259 hydrolysis under typical tropospheric conditions (*Chang et al.*, 2011; *Wang et al.*, 2017).  
260 Through integrating the rate equations, as listed in SI text S1, the solution for aqueous phase  
261 production of  $\text{HNO}_3$  can be obtained (*Seinfeld and Pandis*, 2006):

$$262 \quad [\text{HNO}_3] = \frac{[\text{NO}_x]}{2} \left\{ 1 + \frac{1}{\tau_{\text{NO}_x} - \tau_{\text{N}_2\text{O}_5}} \left[ \tau_{\text{N}_2\text{O}_5} \exp\left(-\frac{t}{\tau_{\text{N}_2\text{O}_5}}\right) - \tau_{\text{NO}_x} \exp\left(-\frac{t}{\tau_{\text{NO}_x}}\right) \right] \right\}$$

263 Thus, the conversion of  $\text{NO}_x$  to  $\text{HNO}_3$  through the hydrolysis of  $\text{N}_2\text{O}_5$  depends on the

264 two lifetimes  $\tau_{NO_x}$  and  $\tau_{N_2O_5}$ , as defined by the reaction kinetics (SI text S1). The key  
265 reaction that formed aqueous phase nitrate is related to the effective reaction of  $N_2O_5$  on the  
266 surface of wet aerosol or droplets (Holmes *et al.*, 2019), and therefore, depends on the  
267 concentration of  $NO_2$  and  $O_3$  ( $[NO_2][O_3]$ ), the available aerosol/droplet SA, and temperature.  
268 Besides the reaction kinetics, temperature could also have influence on the hydrolysis of  
269  $N_2O_5$  (Chang *et al.*, 2011; Chen *et al.*, 2018).

270 As shown in Fig. 3, the theoretically calculated in-cloud nitrate production assuming a  
271 typical uptake coefficient of  $N_2O_5$   $\gamma = 0.06$  (Seinfeld and Pandis, 2006) could well match the  
272 measured nitrate concentrations well ( $R^2 = 0.38$  and  $0.60$  with  $p < 0.01$  for daytime and  
273 nighttime, respectively), varying in a wide range of  $\sim 1$  mg  $L^{-1}$  to  $\sim 60$  mg  $L^{-1}$  for 2020 winter.  
274 The correlation coefficients are obviously higher than those predicted using only  $[NO_x][O_3]$   
275 ( $R^2 = 0$  and  $0.54$  for daytime and nighttime, respectively). This is consistent with previous  
276 results that the nighttime production of  $N_2O_5$  and  $HNO_3$  would be proportional to the  
277 concentration of  $NO_2$  and  $O_3$  ( $[NO_2][O_3]$ ) when assuming  $N_2O_5$  and the  $NO_3$  radical are both  
278 in steady state considering their short lifetimes (Wang *et al.*, 2017; Li *et al.*, 2018). The result  
279 also highlights the significance of SA in the in-cloud  $N_2O_5$  hydrolysis in the build-up of  
280 nitrate through in-cloud processing, even during the daytime. A further comparison of  
281  $[NO_x][O_3]$  and SA for the cloud events and cloud free periods, as shown in Fig. S5, also  
282 supports the above discussion that the higher fraction of nitrate cannot be well explained by  
283 the variations of  $[NO_x][O_3]$ , but rather by the enhanced SA due to the presence of droplets  
284 (Fig. S5b), which is  $> 5$  times on average that for aerosol particles during cloud-free periods.

285 In the present study, the average LWC of cloud droplets is at a level of  $\sim 10^5 \mu\text{g m}^{-3}$ , 3-4  
286 magnitude higher than those for urban haze conditions. As previously reported, high aerosol  
287 LWC (campaign average at  $\sim 50 \mu\text{g m}^{-3}$ ) induced fast heterogeneous uptake coefficient of  
288  $\text{N}_2\text{O}_5$  is prevalent in urban haze (*Chang et al.*, 2011; *Wang et al.*, 2017), and results in  
289 enhanced nitrate in highly humid condition (*Neuman et al.*, 2003; *Pathak et al.*, 2009; *Wang*  
290 *et al.*, 2009).

291 The theoretical estimate indicates that the hydrolysis of  $\text{N}_2\text{O}_5$  may substantially  
292 contribute to the in-cloud production of nitrate even during the daytime, consistent with the  
293 observation results as discussed in Section 3.1. It is also noted that theoretically predicted  
294 nitrate production from the hydrolysis of  $\text{N}_2\text{O}_5$  represents  $\sim 5\text{-}10\%$  of the measured nitrate  
295 (Fig. 3) based on our assumption. It explains  $\sim 1\text{-}3\%$  increase in the nitrate mass fraction in  
296 clouds, whereas the in-cloud processing contributed to  $> 5\%$  increase (Fig. 1). One reason is  
297 that the assumed  $\gamma = 0.06$  might not be representative for  $\text{N}_2\text{O}_5$  uptake in cloud droplets. It  
298 is likely not a major reason since the previously reported  $\gamma$  for liquid water was generally of  
299 the same magnitude, although some higher  $\gamma$  (0.2-0.4) was also observed for deliquescent  
300 sodium sulfate particles (*Sander et al.*, 2015). Another reason is that the SA estimated by the  
301 size distribution data of cloud residues obtained by the GCVI-SMPS only represents part ( $<$   
302 50%) of the cloud droplets, as GCVI was set to sample droplets larger than 8.0  $\mu\text{m}$  in the  
303 present study.

304 Furthermore, a simplified regression and a random forest analysis are also performed  
305 for the high-time resolved RPAs of nitrate obtained by the SPAMS, with  $[\text{NO}_x][\text{O}_3]$ , SA,

306 and temperature as inputs, separated for the cloud RES and cloud-free particles, as detailed  
307 in SI text S2. Note that the concentration of NO<sub>x</sub> is used here to replace the concentration of  
308 NO<sub>2</sub>, since most of NO data were not available for the 2018 spring. The effect should be  
309 limited since NO could be negligible when the air masses are dominantly attributed to long  
310 range transport, which could also be supported by the data (NO, ~0.1 μg m<sup>-3</sup>, < 2% of NO<sub>2</sub>  
311 concentration) in 2020 winter. As expected, the nitrate RPA in the cloud RES particles is  
312 highly correlated to the predicted ones ( $R^2 = 0.75$  and  $0.71$  with  $p < 0.01$  for daytime and  
313 nighttime, respectively), even during the daytime (**Fig. 4**). An inclusion of temperature and  
314 SA in the model substantially improves the correlation coefficient  $R^2$ , which is originally  
315 0.16 and 0.31 between the nitrate RPA and [NO<sub>x</sub>][O<sub>3</sub>] for daytime and nighttime,  
316 respectively. Similarly, the correlation coefficients ( $R^2 = 0.45$  and  $0.66$  for daytime and  
317 nighttime, respectively) are lower for 2018 spring than 2020 winter, without the availability  
318 of SA data. The results are generally consistent with those obtained from random forest  
319 analysis, as shown in Fig. S6. Without the input of SA, [NO<sub>x</sub>][O<sub>3</sub>] and temperature only  
320 explains 52-61% of the observed nitrate RPA for cloud residual particles in 2018 spring,  
321 compared with 72-80% in 2020 winter. Compared with the cloud residual particles, the  
322 predictions for the nitrate RPA in the cloud-free particles are of lower coefficients. Such  
323 difference between the cloud residual and cloud-free particles also reflects the critical role  
324 of SA in the hydrolysis of N<sub>2</sub>O<sub>5</sub> in cloud droplets.

325

### 326 **3.3. Relative importance of N<sub>2</sub>O<sub>5</sub> hydrolysis pathway to nitrate in clouds**

327 The relative contribution of nitrate formation in cloud droplets and cloud-free particles  
328 is also assessed using the CAPRAM model, as shown in Fig. 5. The relative contribution  
329 difference between the cloud droplets and cloud-free particles is primarily attributed to the  
330 different LWC setting, which is tightly linked to the cloud droplets' SA. Furthermore, the  
331 comparison between cloud scenarios with different LWC setting ( $0.05 \text{ g m}^{-3}$  versus  $0.15 \text{ g}$   
332  $\text{m}^{-3}$ ) also shows an enhanced contribution of  $\text{N}_2\text{O}_5$  hydrolysis to nitrate with increasing LWC.  
333 The result supports the above discussion that SA substantially facilitates the hydrolysis of  
334  $\text{N}_2\text{O}_5$ .

335 Nitrate is known to form predominantly by the hydrolysis of  $\text{N}_2\text{O}_5$  (> 80%) for both the  
336 cloud droplets and cloud-free particles for the nighttime. However, both Fig. 3 and Fig. 4  
337 indicate the potential importance of the heterogeneous  $\text{N}_2\text{O}_5$  hydrolysis to nitrate formation  
338 during the daytime. This is likely attributed to the substantial attenuation of the incident solar  
339 radiation by clouds, in which the visibility was as low as < 0.1 km over this study. Previous  
340 studies have also indicated the effect of clouds in the vertical redistribution of the  
341 photochemical activity (Liu *et al.*, 2006; Hall *et al.*, 2018). Most comparatively, Brown *et al.*  
342 (2016) observed a discrepancy between the modelled and observed  $\text{N}_2\text{O}_5$  during a daytime  
343 fog episode in Hong Kong, and attributed to the uptake of  $\text{N}_2\text{O}_5$  to fog droplets. Their  
344 calculation infers that daytime production of soluble nitrate via  $\text{N}_2\text{O}_5$  can be substantially  
345 faster than photochemical conversion through  $\text{OH}+\text{NO}_2$  in the polluted fog episodes (Brown  
346 *et al.*, 2016).

347 The model results in Fig. 5 with the consideration of photolysis rate are, to some extent,

348 consistent with our observations. The overall contribution of  $\text{N}_2\text{O}_5$  hydrolysis pathways  
349 increases by ~20% (from ~50-60% to ~70-80%) when the photolysis rate is reduced to 30%  
350 of the default setting. For daytime only, the contribution of this pathway also increase from  
351 nearly 0 to ~20% during noon hours and ~40% for morning hours. A similar model study  
352 also indicates that  $\text{N}_2\text{O}_5$  hydrolysis contributed to 30% of daytime nitrate formation at Mt.  
353 Tai.(*Zhu et al.*, 2020) Attributed to the substantial attenuation of incident solar radiation by  
354 clouds and high loading of  $\text{PM}_{2.5}$ , the daytime  $\text{N}_2\text{O}_5$  hydrolysis has also been observed to be  
355 an important formation pathway for nitrate in the haze episodes in Xi'an (China), increased  
356 from 8.2% to 20.5% of the total nitrate over 14:00–16:00 by further model simulation,(*Wu*  
357 *et al.*, 2021) and contributed ~10% of nitrate in the north China plain during daytime in  
358 winter (*Liu et al.*, 2020a). Note that our model calculation represents a rough estimation of  
359 relative contribution to the formation of nitrate, since biogenic volatile organic compounds  
360 (which are not available or considered in our model calculation) could also have a potentially  
361 important impact on nitrate formation through affecting the oxidant concentrations  
362 (*Aksoyoglu et al.*, 2017; *Zhang et al.*, 2019), yet remains to be quantified.

363

#### 364 **4. Conclusions and atmospheric implications**

365 The presented results provide direct evidence that in-cloud aqueous processing, in  
366 particular, the hydrolysis of  $\text{N}_2\text{O}_5$  contributing to the enhanced nitrate in cloud residues. We  
367 highlight that hydrolysis of  $\text{N}_2\text{O}_5$  serves as the critical route for the in-cloud formation of  
368 nitrate, even during the daytime. The dependence of in-cloud nitrate formation on cloud

369 droplets' SA extends the observation that higher RH facilitates the formation of nitrate in wet  
370 aerosols (*Neuman et al.*, 2003; *Pathak et al.*, 2009; *Wang et al.*, 2009). Our results would  
371 also help constrain the model simulation (*Holmes et al.*, 2019), as global model studies  
372 disagree on the relative importance of processes contributing to nitrate production in cloud.  
373 There are also studies neglecting  $\text{N}_2\text{O}_5$  and  $\text{NO}_3$  uptake in clouds (*Alexander et al.*, 2009; *Xu*  
374 *and Penner*, 2012; *Hauglustaine et al.*, 2014). Given that  $\text{N}_2\text{O}_5$  hydrolysis acts as a major  
375 sink of  $\text{NO}_x$  in the atmosphere (*Yan et al.*, 2019), further model updates may improve our  
376 understanding on the global dominant nitrate-production pathways and the feedback that  
377 reduces the effectiveness of air pollution mitigation (*Alexander et al.*, 2020; *Chan et al.*,  
378 2021). In addition, significant hydrolysis of  $\text{N}_2\text{O}_5$  in cloud may also pose substantial effect  
379 on the tropospheric ozone budget (*Riemer et al.*, 2003; *Voulgarakis et al.*, 2009; *Strode et al.*,  
380 2017), which needs further investigation.

381 Our results also indicate that in-cloud formed nitrate remains in particulate phase after  
382 cloud evaporation (Fig. S7), changing the mixing state of individual particles. Enhanced  
383 aerosol nitrate is expected to have higher hygroscopicity after cloud evaporation (*Hodas et*  
384 *al.*, 2014; *Sun et al.*, 2018), and therefore, an increase of the particles' ability to act as cloud  
385 condensation nuclei after their cloud passage (*Roth et al.*, 2016). This is different from that  
386 observed in California coast that the nitrate-to-sulfate mass ratio decreases rapidly with  
387 cloud height, due to the volatilization during drop evaporation pushes  $\text{NO}_3$  to the gas phase  
388 (*Prabhakar et al.*, 2014). In addition, vertical turbulent mixing of the residual aerosols from  
389 evaporating cloud droplets may contribute to the nitrate aerosol loading during the daytime

390 at the ground level (*Tao et al.*, 2018).

391 As sulfate is reduced in the future through emission controls (*Chu et al.*, 2020; *Li et al.*,  
392 2020a), higher nitrate fraction is expected through cloud cycling (*Li et al.*, 2020a), which  
393 might also contribute to cloud acidification (*Guo et al.*, 2012). The observational evidence  
394 of a rising trend of nitrate in cloud has been previously reported for the California's San  
395 Joaquin Valley (*Herckes et al.*, 2007; *Herckes et al.*, 2015). It is also noted that the limited  
396 dependence of nitrate formation on the  $[\text{NO}_x][\text{O}_3]$  in the cloud suggest a possibility that  
397 controlling  $\text{NO}_x$  and  $\text{O}_3$  might be offset in the cloudy regions. Given the significance of both  
398 emission and deposition on the variations of nitrate (*Zhai et al.*, 2021) and the contribution  
399 of the transported  $\text{NO}_x$  and  $\text{O}_3$  to the notable effect and complex process of cross-regional  
400 nitrate formation (*Qu et al.*, 2021), knowledge of the in-cloud formation of nitrate would  
401 also benefit  $\text{PM}_{2.5}$  pollution control target over a larger scale.

402 **Data availability**

403 Data used in this paper will be uploaded to Zenodo after the paper is accepted.

404 **Competing interests**

405 The authors declare that they have no conflict of interest.

406 **Author contribution**

407 **Xinhui Bi and Guohua Zhang:** conceptualization, methodology, formal analysis, resource,  
408 writing-original draft, writing-review & editing; **Xiaodong Hu and Wei Sun:** methodology,  
409 investigation, formal analysis, writing-original draft; **Yuxiang Yang, Ziyong Guo, Yuzhen Fu:**  
410 investigation; **Haichao Wang, Shengzhen Zhou, Zongbo Shi:** investigation; supervision;  
411 **Duohong Chen, Lei Li, Mingjin Tang and Xinming Wang:** resource.

412

413 **Financial support**

414 This work was funded by the Natural Science Foundation of Guangdong Province  
415 (2019B151502022), National Natural Science Foundation of China (42077322, 41775124, and  
416 41877307), Youth Innovation Promotion Association CAS (2021354), and Guangdong  
417 Foundation for Program of Science and Technology Research (2019B121205006 and  
418 2020B1212060053).

419 **Acknowledgement**

420 Thanks to Prof. Likun Xue (Shandong University) and Dr. Liang Wen (Leibniz Institute for  
421 Tropospheric Research) for their support of the box modeling of nitrate formation in cloud.

422 **References**

- 423 Aksoyoglu, S., G. Ciarelli, I. El-Haddad, U. Baltensperger, and A. S. H. Prevot (2017),  
424 Secondary inorganic aerosols in Europe: sources and the significant influence of biogenic VOC  
425 emissions, especially on ammonium nitrate, *Atmos. Chem. Phys.*, *17*(12), 7757-7773,  
426 doi:10.5194/acp-17-7757-2017.
- 427 Alexander, B., M. G. Hastings, D. J. Allman, J. Dachs, J. A. Thornton, and S. A. Kunasek (2009),  
428 Quantifying atmospheric nitrate formation pathways based on a global model of the oxygen  
429 isotopic composition ( $\Delta^{17}\text{O}$ ) of atmospheric nitrate, *Atmos. Chem. Phys.*, *9*(14), 5043-5056,  
430 doi:10.5194/acp-9-5043-2009.
- 431 Alexander, B., T. Sherwen, C. D. Holmes, J. A. Fisher, Q. Chen, M. J. Evans, and P. Kasibhatla  
432 (2020), Global inorganic nitrate production mechanisms: comparison of a global model with  
433 nitrate isotope observations, *Atmos. Chem. Phys.*, *20*(6), 3859-3877, doi:10.5194/acp-20-3859-  
434 2020.
- 435 Bauer, S. E., D. Koch, N. Unger, S. M. Metzger, D. T. Shindell, and D. G. Streets (2007), Nitrate  
436 aerosols today and in 2030: a global simulation including aerosols and tropospheric ozone,  
437 *Atmos. Chem. Phys.*, *7*(19), 5043-5059, doi:10.5194/acp-7-5043-2007.
- 438 Bi, X. H., et al. (2016), In situ detection of the chemistry of individual fog droplet residues in  
439 the Pearl River Delta region, China, *J. Geophys. Res.-Atmos.*, *121*(15), 9105-9116,  
440 doi:10.1002/2016JD024886.
- 441 Boone, E. J., A. Laskin, J. Laskin, C. Wirth, P. B. Shepson, B. H. Stirm, and K. A. Pratt (2015),  
442 Aqueous Processing of Atmospheric Organic Particles in Cloud Water Collected via Aircraft  
443 Sampling, *Environ. Sci. Technol.*, *49*(14), 8523-8530, doi:10.1021/acs.est.5b01639.
- 444 Brown, S. S., et al. (2016), Nighttime chemistry at a high altitude site above Hong Kong, *J.*  
445 *Geophys. Res.-Atmos.*, *121*(5), 2457-2475, doi:10.1002/2015JD024566.
- 446 Chan, Y.-C., et al. (2021), Heterogeneous Nitrate Production Mechanisms in Intense Haze  
447 Events in the North China Plain, *J. Geophys. Res.-Atmos.*, *126*(9), doi:10.1029/2021jd034688.
- 448 Chang, W. L., P. V. Bhave, S. S. Brown, N. Riemer, J. Stutz, and D. Dabdub (2011),  
449 Heterogeneous Atmospheric Chemistry, Ambient Measurements, and Model Calculations of

- 450 N<sub>2</sub>O<sub>5</sub>: A Review, *Aerosol Sci. Tech.*, 45(6), 665-695, doi:10.1080/02786826.2010.551672.
- 451 Chen, X., et al. (2020), Field Determination of Nitrate Formation Pathway in Winter Beijing,  
452 *Environ. Sci. Technol.*, 54(15), 9243-9253, doi:10.1021/acs.est.0c00972.
- 453 Chen, Y., R. Wolke, L. Ran, W. Birmili, G. Spindler, W. Schroder, H. Su, Y. F. Cheng, I. Tegen,  
454 and A. Wiedensohler (2018), A parameterization of the heterogeneous hydrolysis of N<sub>2</sub>O<sub>5</sub> for  
455 mass-based aerosol models: improvement of particulate nitrate prediction, *Atmos. Chem. Phys.*,  
456 18(2), 673-689, doi:10.5194/acp-18-673-2018.
- 457 Chu, B., et al. (2020), Air Pollutant Correlations in China: Secondary Air Pollutant Responses  
458 to NO<sub>x</sub> and SO<sub>2</sub> Control, *Environ. Sci. Tech. Lett.*, 7(10), 695-700,  
459 doi:10.1021/acs.estlett.0c00403.
- 460 Draxler, R. R., and G. D. Rolph (2012), *HYSPLIT (HYbrid Single-Particle Lagrangian*  
461 *Integrated Trajectory) Model access via NOAA ARL READY Website*  
462 (<http://ready.arl.noaa.gov/HYSPLIT.php>), MD, Silver Spring.
- 463 Drewnick, F., J. Schneider, S. S. Hings, N. Hock, K. Noone, A. Targino, S. Weimer, and S.  
464 Borrmann (2007), Measurement of ambient, interstitial, and residual aerosol particles on a  
465 mountaintop site in central Sweden using an aerosol mass spectrometer and a CVI, *J. Atmos.*  
466 *Chem.*, 56(1), 1-20, doi:10.1007/s10874-006-9036-8.
- 467 Ervens, B. (2015), Modeling the Processing of Aerosol and Trace Gases in Clouds and Fogs,  
468 *Chem. Rev.*, 115(10), 4157-4198, doi:10.1021/cr5005887.
- 469 Ervens, B., et al. (2003), CAPRAM 2.4 (MODAC mechanism): An extended and condensed  
470 tropospheric aqueous phase mechanism and its application, *J. Geophys. Res.-Atmos.*, 108(D14),  
471 doi:10.1029/2002jd002202.
- 472 Fahey, K. M., S. N. Pandis, J. L. Collett, and P. Herckes (2005), The influence of size-dependent  
473 droplet composition on pollutant processing by fogs, *Atmos. Environ.*, 39(25), 4561-4574,  
474 doi:10.1016/j.atmosenv.2005.04.006.
- 475 Fan, M. Y., Y. L. Zhang, Y. C. Lin, Y. Hong, Z. Y. Zhao, F. Xie, W. Du, F. Cao, Y. Sun, and P.  
476 Fu (2021), Important Role of NO<sub>3</sub> Radical to Nitrate Formation Aloft in Urban Beijing: Insights  
477 from Triple Oxygen Isotopes Measured at the Tower, *Environ. Sci. Technol.*,  
478 doi:10.1021/acs.est.1c02843.

- 479 Fu, X., T. Wang, J. Gao, P. Wang, Y. Liu, S. Wang, B. Zhao, and L. Xue (2020), Persistent Heavy  
480 Winter Nitrate Pollution Driven by Increased Photochemical Oxidants in Northern China,  
481 *Environ. Sci. Technol.*, *54*(7), 3881-3889, doi:10.1021/acs.est.9b07248.
- 482 Guo, J., et al. (2012), Characterization of cloud water chemistry at Mount Tai, China: Seasonal  
483 variation, anthropogenic impact, and cloud processing, *Atmos. Environ.*, *60*, 467-476,  
484 doi:10.1016/j.atmosenv.2012.07.016.
- 485 Guo, S., et al. (2014), Elucidating severe urban haze formation in China, *Proc. Natl. Acad. Sci.*  
486 *USA*, *111*(49), 17373, doi:10.1073/pnas.1419604111.
- 487 Hall, S. R., et al. (2018), Cloud impacts on photochemistry: building a climatology of photolysis  
488 rates from the Atmospheric Tomography mission, *Atmos. Chem. Phys.*, *18*(22), 16809-16828,  
489 doi:10.5194/acp-18-16809-2018.
- 490 Hao, L., et al. (2013), Aerosol Chemical Composition in Cloud Events by High Resolution  
491 Time-of-Flight Aerosol Mass Spectrometry, *Environ. Sci. Technol.*, *47*(6), 2645-2653,  
492 doi:10.1021/es302889w.
- 493 Hauglustaine, D. A., Y. Balkanski, and M. Schulz (2014), A global model simulation of present  
494 and future nitrate aerosols and their direct radiative forcing of climate, *Atmos. Chem. Phys.*,  
495 *14*(20), 11031-11063, doi:10.5194/acp-14-11031-2014.
- 496 Hayden, K. L., A. M. Macdonald, W. Gong, D. Toom-Sauntry, K. G. Anlauf, A. Leithead, S. M.  
497 Li, W. R. Leitch, and K. Noone (2008), Cloud processing of nitrate, *J. Geophys. Res.-Atmos.*,  
498 *113*(D18), 1-18, doi:10.1029/2007jd009732.
- 499 Healy, R. M., et al. (2013), Quantitative determination of carbonaceous particle mixing state in  
500 Paris using single-particle mass spectrometer and aerosol mass spectrometer measurements,  
501 *Atmos. Chem. Phys.*, *13*(18), 9479-9496, doi:10.5194/acp-13-9479-2013.
- 502 Herckes, P., H. Chang, T. Lee, and J. L. Collett (2007), Air pollution processing by radiation  
503 fogs, *Water Air Soil Pollut.*, *181*(1-4), 65-75, doi:10.1007/s11270-006-9276-x.
- 504 Herckes, P., A. R. Marcotte, Y. Wang, and J. L. Collett (2015), Fog composition in the Central  
505 Valley of California over three decades, *Atmos. Res.*, *151*, 20-30,  
506 doi:10.1016/j.atmosres.2014.01.025.
- 507 Hodas, N., A. P. Sullivan, K. Skog, F. N. Keutsch, J. L. Collett, Jr., S. Decesari, M. C. Facchini,

- 508 A. G. Carlton, A. Laaksonen, and B. J. Turpin (2014), Aerosol liquid water driven by  
509 anthropogenic nitrate: implications for lifetimes of water-soluble organic gases and potential for  
510 secondary organic aerosol formation, *Environ. Sci. Technol.*, *48*(19), 11127-11136,  
511 doi:10.1021/es5025096.
- 512 Holmes, C. D., T. H. Bertram, K. L. Confer, K. A. Grahams, A. C. Ronan, C. K. Wirks, and V.  
513 Shah (2019), The Role of Clouds in the Tropospheric NO<sub>x</sub> Cycle: A New Modeling Approach  
514 for Cloud Chemistry and Its Global Implications, *Geophys. Res. Lett.*, *46*(9), 4980-4990,  
515 doi:10.1029/2019gl081990.
- 516 Huang, D. D., Q. Zhang, H. H. Y. Cheung, L. Yu, S. Zhou, C. Anastasio, J. D. Smith, and C. K.  
517 Chan (2018), Formation and Evolution of aqSOA from Aqueous-Phase Reactions of Phenolic  
518 Carbonyls: Comparison between Ammonium Sulfate and Ammonium Nitrate Solutions,  
519 *Environ. Sci. Technol.*, *52*(16), 9215-9224, doi:10.1021/acs.est.8b03441.
- 520 Jeong, C. H., M. L. McGuire, K. J. Godri, J. G. Slowik, P. J. G. Rehbein, and G. J. Evans (2011),  
521 Quantification of aerosol chemical composition using continuous single particle measurements,  
522 *Atmos. Chem. Phys.*, *11*(14), 7027-7044, doi:10.5194/acp-11-7027-2011.
- 523 Kaur, R., and C. Anastasio (2017), Light absorption and the photoformation of hydroxyl radical  
524 and singlet oxygen in fog waters, *Atmos. Environ.*, *164*, 387-397,  
525 doi:10.1016/j.atmosenv.2017.06.006.
- 526 Leaitch, W. R., J. W. Bottenheim, and J. W. Strapp (1988), Possible contribution of N<sub>2</sub>O<sub>5</sub>  
527 scavenging to HNO<sub>3</sub> observed in winter stratiform cloud, *J. Geophys. Res.-Atmos.*, *93*(D10),  
528 12569-12584, doi:10.1029/JD093iD10p12569.
- 529 Li, H. Y., Q. Zhang, B. Zheng, C. R. Chen, N. N. Wu, H. Y. Guo, Y. X. Zhang, Y. X. Zheng, X.  
530 Li, and K. B. He (2018), Nitrate-driven urban haze pollution during summertime over the North  
531 China Plain, *Atmos. Chem. Phys.*, *18*(8), 5293-5306, doi:10.5194/acp-18-5293-2018.
- 532 Li, L., et al. (2011), Real time bipolar time-of-flight mass spectrometer for analyzing single  
533 aerosol particles, *Intl. J. Mass. Spectrom.*, *303*(2-3), 118-124, doi:10.1016/j.ijms.2011.01.017.
- 534 Li, S., et al. (2020a), Characterizing the ratio of nitrate to sulfate in ambient fine particles of  
535 urban Beijing during 2018–2019, *Atmos. Environ.*, 117662,  
536 doi:10.1016/j.atmosenv.2020.117662.

- 537 Li, T., et al. (2020b), Chemical characteristics of cloud water and the impacts on aerosol  
538 properties at a subtropical mountain site in Hong Kong SAR, *Atmos. Chem. Phys.*, *20*(1), 391-  
539 407, doi:10.5194/acp-20-391-2020.
- 540 Lin, Q., et al. (2017), In situ chemical composition measurement of individual cloud residue  
541 particles at a mountain site, southern China, *Atmos. Chem. Phys.*, *17*(13), 8473-8488,  
542 doi:10.5194/acp-17-8473-2017.
- 543 Lin, Y. C., Y. L. Zhang, M. Yu, M. Y. Fan, F. Xie, W. Q. Zhang, G. Wu, Z. Cong, and G.  
544 Michalski (2021), Formation Mechanisms and Source Apportionments of Airborne Nitrate  
545 Aerosols at a Himalayan-Tibetan Plateau Site: Insights from Nitrogen and Oxygen Isotopic  
546 Compositions, *Environ. Sci. Technol.*, *55*(18), 12261-12271, doi:10.1021/acs.est.1c03957.
- 547 Liu, H. Y., et al. (2006), Radiative effect of clouds on tropospheric chemistry in a global three-  
548 dimensional chemical transport model, *J. Geophys. Res.-Atmos.*, *111*(D20), 18,  
549 doi:10.1029/2005jd006403.
- 550 Liu, L., N. F. Bei, B. Hu, J. R. Wu, S. X. Liu, X. Li, R. N. Wang, Z. R. Liu, Z. X. Shen, and G.  
551 H. Li (2020a), Wintertime nitrate formation pathways in the north China plain: Importance of  
552 N<sub>2</sub>O<sub>5</sub> heterogeneous hydrolysis, *Environ. Pollut.*, *266*, 10, doi:10.1016/j.envpol.2020.115287.
- 553 Liu, P., C. Ye, C. Xue, C. Zhang, Y. Mu, and X. Sun (2020b), Formation mechanisms of  
554 atmospheric nitrate and sulfate during the winter haze pollution periods in Beijing: gas-phase,  
555 heterogeneous and aqueous-phase chemistry, *Atmos. Chem. Phys.*, *20*(7), 4153-4165,  
556 doi:10.5194/acp-20-4153-2020.
- 557 Lu, K., et al. (2019), Fast Photochemistry in Wintertime Haze: Consequences for Pollution  
558 Mitigation Strategies, *Environ. Sci. Technol.*, *53*(18), 10676-10684,  
559 doi:10.1021/acs.est.9b02422.
- 560 McNeill, V. F. (2017), Atmospheric Aerosols: Clouds, Chemistry, and Climate, *Annu. Rev.*  
561 *Chem. Biomol.*, *8*(1), 427-444, doi:10.1146/annurev-chembioeng-060816-101538.
- 562 Neuman, J. A., et al. (2003), Variability in ammonium nitrate formation and nitric acid depletion  
563 with altitude and location over California, *J. Geophys. Res.-Atmos.*, *108*(D17), 12,  
564 doi:10.1029/2003jd003616.
- 565 Pathak, R. K., W. S. Wu, and T. Wang (2009), Summertime PM<sub>2.5</sub> ionic species in four major

- 566 cities of China: nitrate formation in an ammonia-deficient atmosphere, *Atmos. Chem. Phys.*,  
567 9(5), 1711-1722.
- 568 Prabhakar, G., B. Ervens, Z. Wang, L. C. Maudlin, M. M. Coggon, H. H. Jonsson, J. H. Seinfeld,  
569 and A. Sorooshian (2014), Sources of nitrate in stratocumulus cloud water: Airborne  
570 measurements during the 2011 E-PEACE and 2013 NiCE studies, *Atmos. Environ.*, 97, 166-173,  
571 doi:10.1016/j.atmosenv.2014.08.019.
- 572 Pratt, K. A., P. J. DeMott, J. R. French, Z. Wang, D. L. Westphal, A. J. Heymsfield, C. H. Twohy,  
573 A. J. Prenni, and K. A. Prather (2009), In situ detection of biological particles in cloud ice-  
574 crystals, *Nature Geosci.*, 2(6), 397-400.
- 575 Qu, K., et al. (2021), Cross-regional transport of PM<sub>2.5</sub> nitrate in the Pearl River Delta, China:  
576 Contributions and mechanisms, *Sci. Total. Environ.*, 753, doi:10.1016/j.scitotenv.2020.142439.
- 577 Riemer, N., H. Vogel, B. Vogel, B. Schell, I. Ackermann, C. Kessler, and H. Hass (2003), Impact  
578 of the heterogeneous hydrolysis of N<sub>2</sub>O<sub>5</sub> on chemistry and nitrate aerosol formation in the lower  
579 troposphere under photosmog conditions, *J. Geophys. Res.-Atmos.*, 108(D4), 21,  
580 doi:10.1029/2002jd002436.
- 581 Roth, A., J. Schneider, T. Klimach, S. Mertes, D. van Pinxteren, H. Herrmann, and S. Borrmann  
582 (2016), Aerosol properties, source identification, and cloud processing in orographic clouds  
583 measured by single particle mass spectrometry on a central European mountain site during  
584 HCCT-2010, *Atmos. Chem. Phys.*, 16(2), 505-524, doi:10.5194/acp-16-505-2016.
- 585 Sander, S. P., R. R. Friedl, D. M. Golden, M. J. Kurylo, G. K. Moortgat, P. H. Wine, A. R.  
586 Ravishankara, C. E. Kolb, M. J. Molina, and S. Diego (2015), *Chemical kinetics and*  
587 *photochemical data for use in atmospheric studies*, Evaluation No. 14 (JPL Publication 02-25).  
588 National Aeronautics and Space Administration.
- 589 Scharko, N. K., A. E. Berke, and J. D. Raff (2014), Release of Nitrous Acid and Nitrogen  
590 Dioxide from Nitrate Photolysis in Acidic Aqueous Solutions, *Environ. Sci. Technol.*, 48(20),  
591 11991-12001, doi:10.1021/es503088x.
- 592 Schneider, J., S. Mertes, D. van Pinxteren, H. Herrmann, and S. Borrmann (2017), Uptake of  
593 nitric acid, ammonia, and organics in orographic clouds: mass spectrometric analyses of droplet  
594 residual and interstitial aerosol particles, *Atmos. Chem. Phys.*, 17(2), 1571-1593,

- 595 doi:10.5194/acp-17-1571-2017.
- 596 Seinfeld, J. H., and S. N. Pandis (2006), *Atmospheric Chemistry and Physics: From Air*  
597 *Pollution to Climate Change*, John Wiley&Sons, Inc., New Jersey.
- 598 Sellegri, K., P. Laj, A. Marinoni, R. Dupuy, M. Legrand, and S. Preunkert (2003), Contribution  
599 of gaseous and particulate species to droplet solute composition at the Puy de Dome, France,  
600 *Atmos. Chem. Phys.*, *3*, 1509-1522, doi:10.5194/acp-3-1509-2003.
- 601 Shi, X., A. Nenes, Z. Xiao, S. Song, H. Yu, G. Shi, Q. Zhao, K. Chen, Y. Feng, and A. G. Russell  
602 (2019), High-Resolution Data Sets Unravel the Effects of Sources and Meteorological  
603 Conditions on Nitrate and Its Gas-Particle Partitioning, *Environ. Sci. Technol.*, *53*(6), 3048-3057,  
604 doi:10.1021/acs.est.8b06524.
- 605 Shingler, T., et al. (2012), Characterisation and airborne deployment of a new counterflow  
606 virtual impactor inlet, *Atmos. Meas. Tech.*, *5*(6), 1259-1269, doi:10.5194/amt-5-1259-2012.
- 607 Song, X. H., P. K. Hopke, D. P. Fergenson, and K. A. Prather (1999), Classification of single  
608 particles analyzed by ATOFMS using an artificial neural network, ART-2A, *Anal. Chem.*, *71*(4),  
609 860-865.
- 610 Strode, S. A., A. R. Douglass, J. R. Ziemke, M. Manyin, J. E. Nielsen, and L. D. Oman (2017),  
611 A Model and Satellite-Based Analysis of the Tropospheric Ozone Distribution in Clear Versus  
612 Convectively Cloudy Conditions, *J. Geophys. Res.-Atmos.*, *122*(21), 11948-11960,  
613 doi:10.1002/2017jd027015.
- 614 Sultana, C. M., G. C. Cornwell, P. Rodriguez, and K. A. Prather (2017), FATES: a flexible  
615 analysis toolkit for the exploration of single-particle mass spectrometer data, *Atmos. Meas. Tech.*,  
616 *10*(4), 1323-1334, doi:10.5194/amt-10-1323-2017.
- 617 Sun, J. X., et al. (2018), Key Role of Nitrate in Phase Transitions of Urban Particles:  
618 Implications of Important Reactive Surfaces for Secondary Aerosol Formation, *J. Geophys.*  
619 *Res.-Atmos.*, *123*(2), 1234-1243, doi:10.1002/2017JD027264.
- 620 Tao, J., et al. (2018), Observational evidence of cloud processes contributing to daytime elevated  
621 nitrate in an urban atmosphere, *Atmos. Environ.*, *186*, 209-215,  
622 doi:10.1016/j.atmosenv.2018.05.040.
- 623 Tian, M., et al. (2019), Increasing importance of nitrate formation for heavy aerosol pollution

- 624 in two megacities in Sichuan Basin, southwest China, *Environ. Pollut.*, 250, 898-905,  
625 doi:10.1016/j.envpol.2019.04.098.
- 626 Voulgarakis, A., O. Wild, N. H. Savage, G. D. Carver, and J. A. Pyle (2009), Clouds, photolysis  
627 and regional tropospheric ozone budgets, *Atmos. Chem. Phys.*, 9(21), 8235-8246,  
628 doi:10.5194/acp-9-8235-2009.
- 629 Wang, H., et al. (2017), High N<sub>2</sub>O<sub>5</sub> Concentrations Observed in Urban Beijing: Implications of  
630 a Large Nitrate Formation Pathway, *Environ. Sci. Tech. Lett.*, doi:10.1021/acs.estlett.7b00341.
- 631 Wang, X. F., Y. P. Zhang, H. Chen, X. Yang, J. M. Chen, and F. H. Geng (2009), Particulate  
632 Nitrate Formation in a Highly Polluted Urban Area: A Case Study by Single-Particle Mass  
633 Spectrometry in Shanghai, *Environ. Sci. Technol.*, 43(9), 3061-3066, doi:10.1021/es8020155.
- 634 Wen, L., L. K. Xue, X. F. Wang, C. H. Xu, T. S. Chen, L. X. Yang, T. Wang, Q. Z. Zhang, and  
635 W. X. Wang (2018), Summertime fine particulate nitrate pollution in the North China Plain:  
636 increasing trends, formation mechanisms and implications for control policy, *Atmos. Chem.*  
637 *Phys.*, 18(15), 11261-11275, doi:10.5194/acp-18-11261-2018.
- 638 Wu, C., L. Liu, G. Wang, S. Zhang, G. Li, S. Lv, J. Li, F. Wang, J. Meng, and Y. Zens (2021),  
639 Important contribution of N<sub>2</sub>O<sub>5</sub> hydrolysis to the daytime nitrate in Xi'an, China during haze  
640 periods: Isotopic analysis and WRF-Chem model simulation, *Environ. Pollut.*, 117712,  
641 doi:<https://doi.org/10.1016/j.envpol.2021.117712>.
- 642 Xiao, H.-W., et al. (2020), Differentiation Between Nitrate Aerosol Formation Pathways in a  
643 Southeast Chinese City by Dual Isotope and Modeling Studies, *J. Geophys. Res.-Atmos.*,  
644 125(13), doi:10.1029/2020jd032604.
- 645 Xu, L., and J. E. Penner (2012), Global simulations of nitrate and ammonium aerosols and their  
646 radiative effects, *Atmos. Chem. Phys.*, 12(20), 9479-9504, doi:10.5194/acp-12-9479-2012.
- 647 Xu, Q., S. Wang, J. Jiang, N. Bhattarai, X. Li, X. Chang, X. Qiu, M. Zheng, Y. Hua, and J. Hao  
648 (2019), Nitrate dominates the chemical composition of PM<sub>2.5</sub> during haze event in Beijing,  
649 China, *Sci. Total. Environ.*, 689, 1293-1303, doi:10.1016/j.scitotenv.2019.06.294.
- 650 Yan, C., Y. J. Tham, Q. Z. Zha, X. F. Wang, L. K. Xue, J. N. Dai, Z. Wang, and T. Wang (2019),  
651 Fast heterogeneous loss of N<sub>2</sub>O<sub>5</sub> leads to significant nighttime NO<sub>x</sub> removal and nitrate aerosol  
652 formation at a coastal background environment of southern China, *Sci. Total. Environ.*, 677,

- 653 637-647, doi:10.1016/j.scitotenv.2019.04.389.
- 654 Ye, C., D. E. Heard, and L. K. Whalley (2017a), Evaluation of Novel Routes for NO<sub>x</sub> Formation  
655 in Remote Regions, *Environ. Sci. Technol.*, *51*(13), 7442-7449, doi:10.1021/acs.est.6b06441.
- 656 Ye, C., N. Zhang, H. Gao, and X. Zhou (2017b), Photolysis of Particulate Nitrate as a Source of  
657 HONO and NO<sub>x</sub>, *Environ. Sci. Technol.*, *51*(12), 6849-6856, doi:10.1021/acs.est.7b00387.
- 658 Zhai, S., et al. (2021), Control of particulate nitrate air pollution in China, *Nature Geosci.*, *14*(6),  
659 389-395, doi:10.1038/s41561-021-00726-z.
- 660 Zhang, G. H., et al. (2017), Insight into the in-cloud formation of oxalate based on in situ  
661 measurement by single particle mass spectrometry, *Atmos. Chem. Phys.*, *17*(22), 13891-13901,  
662 doi:10.5194/acp-17-13891-2017.
- 663 Zhang, J., S. Lance, R. Brandt, J. Marto, M. Ninneman, and J. Schwab (2019), Observed below-  
664 Cloud and Cloud Interstitial Submicron Aerosol Chemical and Physical Properties at Whiteface  
665 Mountain, New York, during August 2017, *Acs Earth Space Chem.*, *3*(8), 1438-1450,  
666 doi:10.1021/acsearthspacechem.9b00117.
- 667 Zhang, R., M. Gen, T. M. Fu, and C. K. Chan (2021), Production of Formate via Oxidation of  
668 Glyoxal Promoted by Particulate Nitrate Photolysis, *Environ. Sci. Technol.*, *55*(9), 5711-5720,  
669 doi:10.1021/acs.est.0c08199.
- 670 Zheng, H., et al. (2020), Contribution of Particulate Nitrate Photolysis to Heterogeneous Sulfate  
671 Formation for Winter Haze in China, *Environ. Sci. Tech. Lett.*, *7*(9), 632-638,  
672 doi:10.1021/acs.estlett.0c00368.
- 673 Zhu, Y., A. Tilgner, E. H. Hoffmann, H. Herrmann, K. Kawamura, L. Yang, L. Xue, and W.  
674 Wang (2020), Multiphase MCM-CAPRAM modeling of the formation and processing of  
675 secondary aerosol constituents observed during the Mt. Tai summer campaign in 2014, *Atmos.*  
676 *Chem. Phys.*, *20*(11), 6725-6747, doi:10.5194/acp-20-6725-2020.
- 677

678 **Figure captions:**

679 **Figure 1.** Box-and-whisker plots of (a) the mass fraction of nitrate in PM<sub>2.5</sub> and cloud  
680 water and (b) the RPA of nitrate separated for the cloud-free, cloud residual particles  
681 (RES), and cloud interstitial particles (INT), in 2018 spring and 2020 winter,  
682 respectively. In a box and whisker plot, the lower, median and upper line of the box  
683 denotes the 25, 50, and 75 percentiles, respectively; the lower and upper edges of the  
684 whisker denote the 10 and 90 percentiles, respectively.

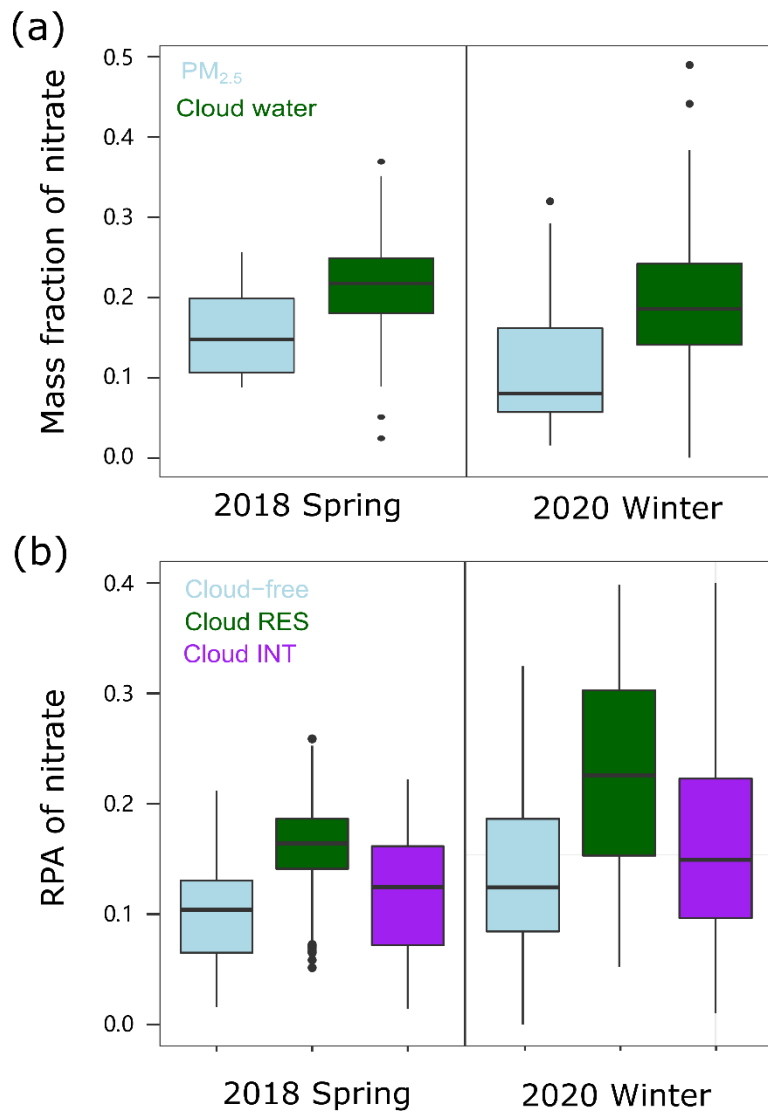
685 **Figure 2.** Size dependent RPA of nitrate and RPA ratio of nitrate/sulfate, separated  
686 for all the detected cloud-free, cloud residual particles (RES), and cloud interstitial  
687 particles (INT), in (a) 2018 spring and (b) 2020 winter, respectively.

688 **Figure 3.** Theoretical calculation of the trend of in-cloud produced nitrate from the  
689 hydrolysis of N<sub>2</sub>O<sub>5</sub> versus the temporal variations of NO<sub>3</sub> concentration in cloud  
690 water in 2020 winter.

691 **Figure 4.** Correlation analysis between the observed RPAs of nitrate and the  
692 predicted RPAs of nitrate, with inputs of NO<sub>2</sub>, O<sub>3</sub> and LWC, for the (a) cloud-free and  
693 (b) cloud residual particles (RES), respectively.

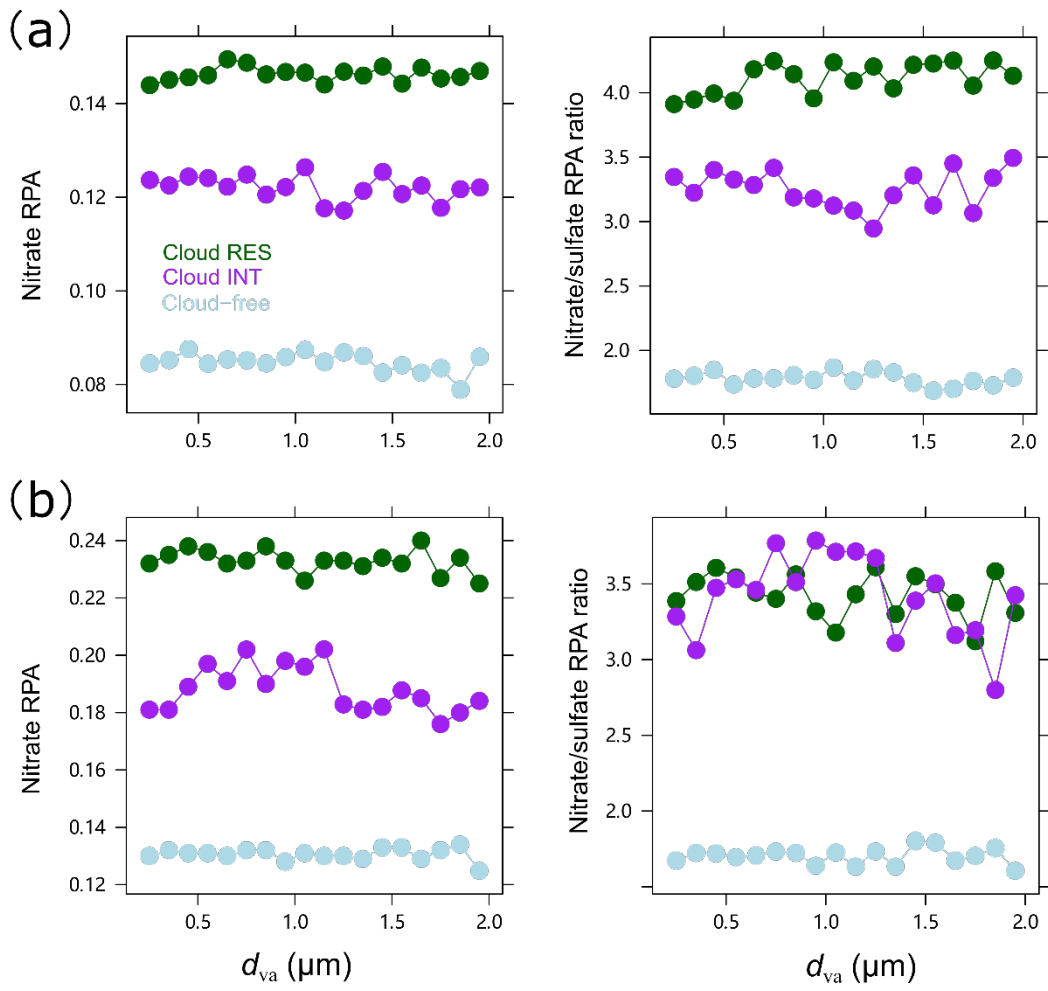
694 **Figure 5.** Relative contribution of each pathway to the nitrate production in wet  
695 aerosols (WA, 0.5 μm) and cloud droplets (CD, 8μm), respectively, simulated by the  
696 RACM-CAPRAM. The atmospheric conditions considered for comparison are LWC

697 (10<sup>-5</sup>-10<sup>-4</sup> g cm<sup>-3</sup> for wet aerosols and 0.05-0.15 g cm<sup>-3</sup>) and photolysis rates (30%,  
698 50%, 100%).



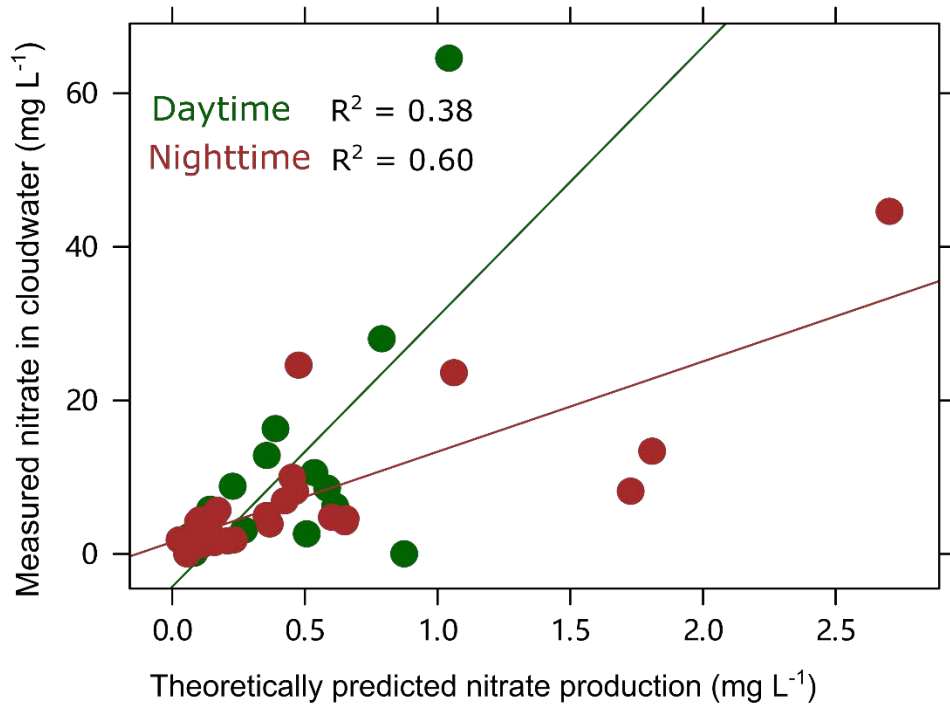
699

700 **Fig. 1.**



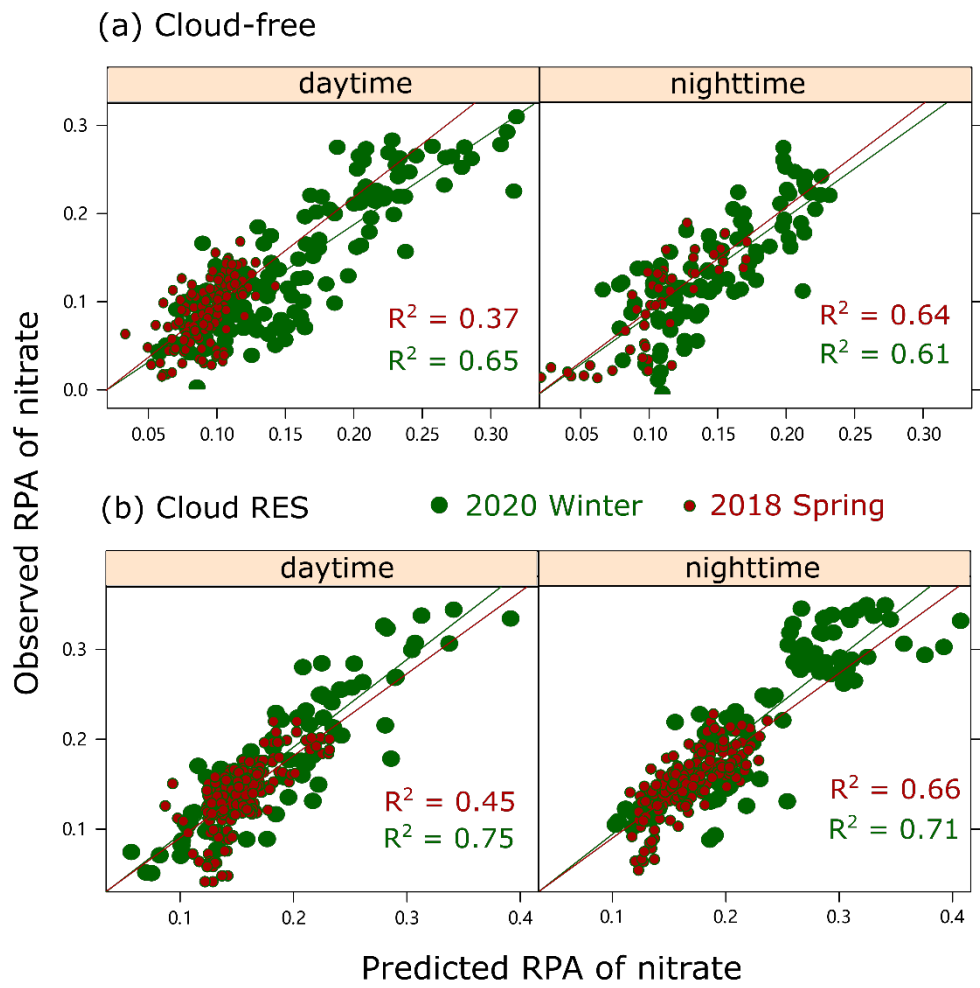
701

702 **Fig. 2.**



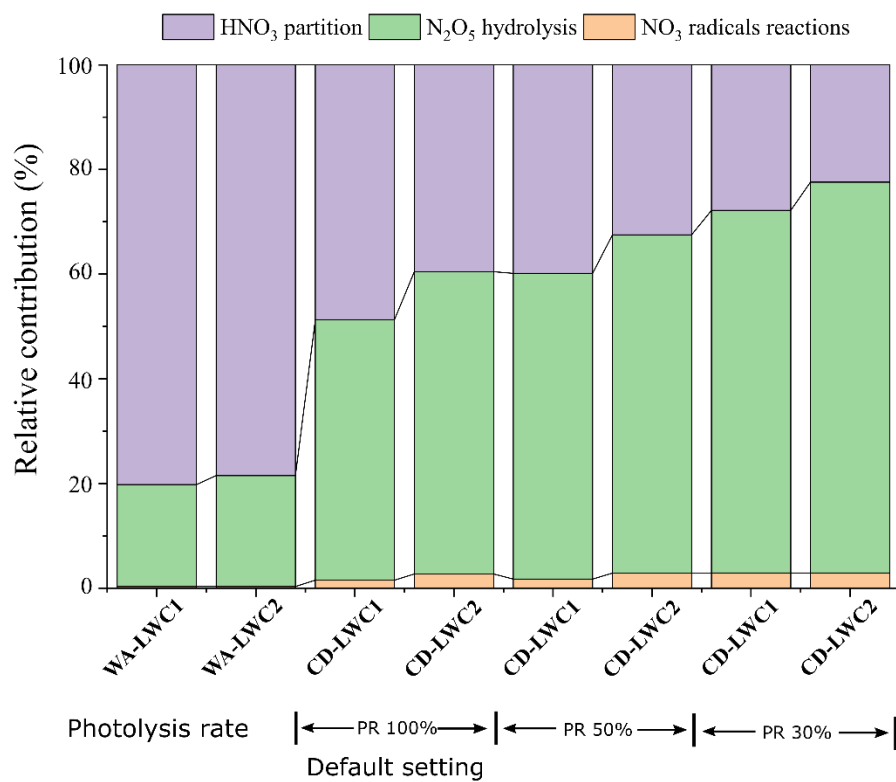
703

704 **Fig. 3.**



705

706 **Fig. 4.**



707

708 **Fig. 5.**